Journal of Materials Chemistry B

Accepted Manuscript

ROYAL SOCIETY OF CHEMISTRY

www.rsc.org/materialsB

Journal Name

ARTICLE

Received 00th January 20xx,

Accepted 00th January 20xx

DOI: 10.1039/x0xx00000x

www.rsc.org/

In situ generation of electron acceptor to amplify the photoelectrochemical signal from poly(dopamine)-sensitized TiO_2 signal crystal for immunoassay

Yilin Li,[a] Hong Dai, *[a] Qingrong Zhang,[a] Shupei Zhang,[a] Sihong Chen,[a] Zhensheng Hong,*[b] and Yanyu Lin[c]

A versatile photoelectrochemical immunoassay protocol was designed for quantitative monitoring the tumor markers by utilizing the poly(dopamine)-sensitized titanium dioxide (TiO_2) signal crystal with the support of ordered mesoporous carbon. Poly(dopamine) was introduced here to alter the optical properties of TiO_2 signal crystal, thereby improving the visible light absorption and photoelectrical responses. More importantly, a new enzyme-like biomimetic catalyst was exploited as the signal amplifier to catalyze the hydroquinone. The generated product was deposited on electrode surface and served as an efficient sacrificial electrons acceptor, which could receive the photo-generated electrons of the excited semiconductor to assist the cathode photocurrent enhancement. Herein, a competitive-type immunosensor was achieved through the biomimetic catalyst labeled prostate specific antigen competing with the target antigen of different concentrations to react with the specific antibody anchored on the poly(dopamine)-sensitized TiO_2 signal crystal. Under optimal conditions, the photocurrent decreased with the increasing target concentration in a dynamic working range from 1×10^{-6} ng/mL to 50 ng/mL, which provided a new photoelectrochemical consideration for tumor markers analysis.

1. Introduction

Immunoassays have stimulated substantial attention with the flourishing development of proteomics and genomics research for applications in food safety, medical diagnosis and clinical surveillance.[1] Prostate cancer is one of the most commonly diagnosed malignancy and prostate specific antigen (PSA) has been recognized as the premier tumor marker for initial monitoring the prostate cancer and recurrence of the disease after treatment. A host of analytical protocols have been reported for monitoring PSA, including the enzyme linked immunosor-bent assay,[2] fluorescence,[3] electrochemical,[4] surface plasmon resonance (SPR),[5] isotope labeling mass spectrometry,[6] and chromatography[7] etc. Nevertheless, a critical demand with simple, accurate, and cost-effective detection technology for earlier and sensitive profiling of cancer biomarkers is still highly desirable. Photoelectrochemical (PEC) immunoassay has obtained substantial intrigue due to its finely attractive performance for future protein assay.[8] This technique possesses higher sensitivity than the electrochemical strategies because of the reduced background signals originated from the different energy forms of the illumination source and determination signal.[9, 10] Presently, most of the signal changes for PEC immunoassays could be concluded into two types: "signal-on" and "signal-off". A multitude of immunoassays belong to the later type owing to the similar designs with quenching function to photo-generated carriers and steric hindrance effect induced by immunized interaction between antigen and antibody. With aim to enhance the sensitivity of PEC immunoassays, enzymes-mediated methodologies are frequently employed for signal amplification, however, introduction of the natural enzyme as labels still faces severe limitations in these "signal-off" PEC platforms. Initially, the sensor preparation cost, storage and testing process are expensive, time-consuming and complicated. From another point of view, the stability of the natural enzyme is inferior, which reduces the reproducibility and accuracy of the designed immuno-sensing platform. Most importantly, in the "signal-off" detection procedure, some potential unfavourable factors such as the latent inhibitors and bias acid-base circumstances could deactivate the activity of the natural enzyme, which causes the unclear outcome for the source of "signal-off" as well as the inconsistent signal response. One promising approach is to exploit a feasible mimetic enzyme system label to bypass these drawbacks. Compared to natural enzymes, artificial enzyme owns several superiorities, such as it is relatively facile for labeling, less expensive to produce, and more resistant to heat treatment and hydrolysis.[11] Until now, limited PEC detection systems based on mimetic enzyme were reported; thus, the realization of an innovative PEC immunoassay by labeling with imitating enzyme for signal amplification would be highly envisioned. Inspired from the research achievement of Wang's

[a] College of Chemistry and Chemical Engineering, Fujian Normal University, Fuzhou, Fujian, 350108,China, Fax: (+86)-591-22866135,*E-mail: dhong@fjnu.edu.cn
[b] Fujian Provincial Key Laboratory of Quantum Manipulation and New Energy Materials, College of Physics and Energy, Fujian Normal University, Fuzhou 350108, P. R. China,*E-mail: winter0514@163.com
[c] Ministry of Education Key Laboratory of Analysis and Detection for Food Safety, and Department of Chemistry, Fuzhou University, Fuzhou 350002, P. R. China.
† Electronic Supplementary Information (ESI) available: See
DOI: 10.1039/x0xx00000x

group, a new-type mimicking enzyme was obtained by chitosan (CS) functioned silver halide nanoparticles, which possessed intrinsic peroxidase-like activity that could be utilized as biomimetic catalyst (BMC) to oxidize the typical substrates.[12] Hence, the development of this BMC-labeled PEC immunoassay might be a valuable route for signal enhancement. Moreover, if this novel BMC were integrated into the mimetic enzyme-labeled PEC strategies, a more widespread perspective for PEC transducer construction would be designed.

Enzymatic biocatalytic precipitation (BCP) was one of the strategies in PEC immunoassay,[13, 14] which involved the in suit formation of indissolvable products on electrode surface via the catalytic by natural or artificial enzymes,[15, 16] thereby altering the photo-generated interfacial electrons transfer. Up to present, infrequent application about the BCP scheme has been reported, let along the exploitation of enzyme mimetic-induced BCP for PEC immunoassays construction. Yet now a new-type BCP alternative method was designed to mediate the photo-response. Hydroquinone (HQ), different from the 4-chloro-1-naphthol, was utilized as the substrate of BMC. During catalysis process, the water-insoluble p-benzoquinone (PBQ) film was formed and deposited on electrode surface in the presence of H_2O_2. Noticeably, the in suit generated PBQ could be utilized as electron acceptor, receiving the electrons from the conduction band (CB) of photoactive materials and improving the cathode photocurrent.

In PEC detection, photoactive materials intimately affect the photoconversion efficiency. Titanium dioxide (TiO_2) single crystals (TSC) emerged as an attractive class of photoactive material has been extensively applied for various optoelectronic fields owing to its particular characteristics: high crystallinity, oriented subunit alignment, light corrosion resistance and versatility in surface modification.[17] While TSC has found its utilization in photocatalysts,[18, 19] solar cell,[20] and gas sensing,[21] rather limited effort exerted on the PEC sensor still needs to be exploited. In addition, owing to the large band gap (3.2 eV for anatase), only ~4% of the incoming solar energy could be utilized by TSC, which restricted its application in PEC bioanalysis. Hence, in this work, a highly biocompatible poly(dopamine) (PDA) was chose as the organic sensitizer to promote the absorption of visible light. And the other vital factor was that PDA could effectively immobilize large amounts of antibody.[22] Messersmith's group has been tested surface-active PDA adhered to plenty of surfaces, including noble metals (Au, Ag), semiconductors (GaAs), and oxides (TiO_2, SiO_2) to form robust dopamine-derived films. The resulting films could support a large quantity of secondary reactions.[23] Qingji Xie's group applied biocomposites with PDA as matrix to support antibody for high-performance sandwich-type immunosensor.[24] In view of the above-mentioned facts, the self-polymerization of dopamine with charged side chains provided a facile one-step functionalization with simple ingredients and mild reaction condition.[25]

In order to further improve the sensitivity of TSC, incorporation of carbonaceous substances with high electrical conductivity has been discovered a way to enhance the photoconversion efficiency of wide band gap semiconductors. Particularly, the ordered mesoporous carbon (OMC) presents an efficient electron transfer rate and larger current response due to the numerous edge-plane-like defect sites and admirable electrical conduction.[26, 27] Therefore, OMC could act as a scaffold in splitting and transferring photo-induced charge carriers, inhibiting the recombination of electron-hole (e^--h^+) pairs of TSC.

Herein, the TSC semiconductor combined with PDA and OMC was used as an excellent photoactive material and sensitizer to promote the photocurrent response. The PEC experimental outcomes revealed that the composites offered remarkable superiorities in strengthening light absorption and fast charge separation, which encouraged photocurrent intensity. In view of the specific recognition between antibody and antigen, an excellent biosensing platform was developed by stepwise modification of OMC, PDA-sensitized TSC, PSA-antibody (Ab) and the mixed solution containing target PSA and PSA-conjugated BMC (PSA@BMC). Its detection mechanism for PSA was illustrated in Scheme 1. Under the negative applied potential, the response of TSC presented cathode photocurrent signal. The formed PDA via self-polymerization could accept photo-induced electrons from the CB of TSC, further enhancing cathodic photocurrent signal. Additionally, the in situ generated water-insoluble PBQ deposition film with abundant electron accepting groups could receive the photo-induced electrons of illuminated TSC/PDA, efficiently elevating charge separation and enhancing cathodic photocurrent. Hence, the BMC labeling as a catalytic amplifier greatly improved sensitivity of this method and the design was totally different from the previous BCP research that only used as inhibitor. It was anticipated that this BCP-dependent BMC with distinctive magnifying function would offer a promising tool for typical bioassay.

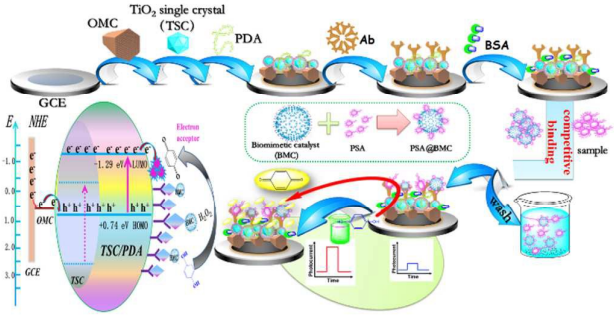

Scheme 1 (A) Fabrication procedure and photocurrent generation mechanism of the PEC immunosensor.

2. Experimental

2.1 Materials and Reagents

PSA and Ab were purchased from Shanghai Linc-Bio Science Co. LTD. Dopamine hydrochloride (98%), glutaraldehyde (GLD, 5.0% aqueous solution), CS, and bovine serum albumin (BSA, 96~99%) were obtained from Aladdin Industrial Corporation (Shanghai, China), Jinshan Tingxin Chemical Plant (Shanghai, China), Sigma (St. Louis, MO, USA), and Biss Inc. (Beijing, China), respectively. The phosphate buffer solution (0.1 M PBS, pH 7.4 and 7.0) was prepared by mixing a stock solution of 0.1 M NaH_2PO_4 and Na_2HPO_4 to adjust the pH value. Deionized (DI) water was prepared of the solution by water purification system (China). OMC was prepared according to

the literature by utilizing solid core/mesoporous shell silica spheres SBA-15 as template.[27]

2.2 Synthesis of BMC for BCP scheme and the preparation of PSA@BMC conjugates

BMC was prepared according to the previously published protocols.[12] Briefly, 3.0 mL of 0.1 M $AgNO_3$ aqueous solution was added in 1.5 mL of 1.0 % (m/v) CS solution and stirred for 0.5 h. Subsequently, 3.0 mL of 0.15 M KI aqueous solution was added into the above solution and stirred for 2 h. Finally, a dispersion containing BMC nanoparticles was generated.

Conjugation of PSA with BMC was achieved by using the classic GLD coupling reaction between amine (-NH_2) groups on the surface of BMC and PSA. Firstly, 30 μL of 5.0% GLD was added to 30 μL BMC solution, diluted by PBS (pH 7.4), stirred for 20 min, and stationarily placed for 4 h at 4 °C. Following that, 35 μL 50 mg/mL PSA was added to the resultant solution and further incubated for 6 h at 4 °C under gentle shaking. Afterwards, the mixture solution was centrifuged at 8000 rpm to remove excess PSA and the obtained bioconjugation was dispersed in PBS (pH 7.4) containing 5 μL BSA (1%), which was stored at 4 °C for 1 h. Finally, the resulting solution was centrifuged at 8000 rpm, removed excess BSA and redispersed in the PBS (pH 7.4) for further use.

2.3 Construction of the competitive PEC immuno-sensor for PSA

Scheme 1 gave the schematic illustration of PEC immunoassay for target PSA by coupling with OMC and PDA co-sensitive TSC as well as BMC-induced electron acceptor for application. PDA was an efficient multifunctional polymer matrix to support PSA antibody. The existence of functional groups (i.e., catechol and amine) on the surface of PDA makes it suitable for further conjugation or modification. Before incubation with Ab (5 μL, 60 ng/mL), the GCE/OMC/TSC/PDA electrode was immersed in 60 μL of GLD solution for 1.5 h to link the -OH groups in PDA and then washed by PBS. The aldehyde group (-CHO) of glutaraldehyde (GLD) could react with the -OH group in PDA via the aldol condensation reaction. After that, the electrode was immersed in Ab solution for 1 h, the Ab could be immobilized on the electrode surface through the GLD crosslinking method that the other –CHO could couple with the -NH_2 groups in Ab. Then this modified electrode was rinsed with PBS (pH 7.4) to remove physically absorbed Ab before blocking with 5 μL of 1.0% BSA for 1 h at 4 °C. Subsequently, the obtained electrode of GCE/OMC/TSC/PDA/Ab was immersed into the mixture solution (60 μL) containing PSA@BMC (30 μL) and PSA standards with different concentrations for an incubation of 1 h at 4 °C followed by rinsing with the PBS (pH 7.4). Finally, the GCE/OMC/TSC/PDA/Ab/PSA@BMC was allowed for incubation at 30 °C for 15 min in the solution consisting of 1.0 mmol/L of HQ and 0.15 mmol/L of H_2O_2. After that, the electrode was rinsed with PBS (pH 7.4) and dried for PEC measurements.

3. Results and Discussion

3.1 Morphology and composition characterization

The morphology of OMC was characterized by SEM and TEM. As shown in Fig. 1A, the ordered mesopore channels of SBA-15 possessed a uniform size, suggesting the template was well synthesized.[28] Exquisitely, the OMC was composed of small grains, which possessed a submicrometer-scale particle size with the length of ca. 0.6~0.8 μm and ca. 10 nm in diameter. To further exploit the structure of OMC, TEM was utilized to investigate the construction (the inset in Fig. 1A), bright stripe-like structures with rough surface were clearly seen on the TEM image, representing the pore-wall images and implying that OMC owned large surface area. The above results demonstrated that OMC could be applied as the photocatalyst support due to its high porosity and large surface area. The morphology of the TSC sample was observed by the SEM image (Fig. 1B), which was consisted of some rhombus-like plates. The TSC/PDA displayed a blurry appearance and morphology of the TSC got irregular (Fig. S3, ESI†).To further confirm the crystal structure of the prepared TSC, Raman spectra were performed to identify the structure (the inset in Fig. 1B), the peak appeared at 144 cm^{-1} was the O-Ti-O bending mode, and this fundamental vibrational feature certified the pure anatase TiO_2 was formed in the products. The other four distinct peaks located at 197, 396, 514 and 637 cm^{-1} were corresponding to the E_g, B_{1g}, A_{1g}+B_{1g} and E_g modes, respectively,[29-31] further verified the anatase phase of the synthesized TSC. Additionally, the BMC nanoproducts were observed by typical TEM images, indicating that they were nanoparticles with diameters of 40~70 nm. Moreover, the HRTEM image (the inset in Fig. 1C) was performed to identify the BMC crystal structure. The lattice fringes with interplanar spacing of 0.353 nm was very close to the (101) lattice plane of hexagonal β-AgI phase (0.351 nm).[32] One possibility was that combining with CS may lightly influenced the interplanar spacing of the (101) planes.

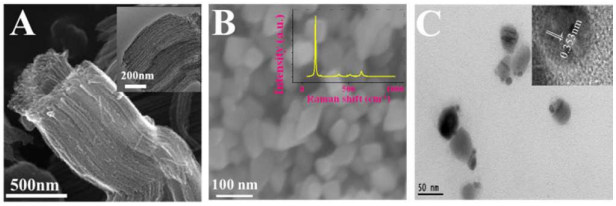

Figure 1 SEM images of OMC (A) and TSC (B); TEM images of BMC (C). The insets in (A), (B) and (C) were TEM image of OMC, Raman spectra of TSC and the HRTEM image of BMC.

3.2 Excellent PEC performance of TSC/PDA

Recently, an intriguing strategy was proposed to change the band gap of the TiO_2 by attaching the oxygen-containing substituents to bind to the TiO_2 nanostructure surface.[33] These biomolecules could alter the coordination environment and endow the nanostructures new hybrid optical properties that was originated from the ligand-to-metal charge transfer interaction between the metal surface atoms and ligand.[34] The pioneering works of Dimitrijevic's and Rajh's groups have proved that modification of enediol ligands on TiO_2 nanomaterials could harvest visible light and improve the efficient spatial separation of charges.[22, 35] Therefore, PDA was introduced here to improve the photoelectric conversion efficiency. A series of PEC measurements were employed to certify this supposition. As depicted in Fig. 2A, TSC/PDA submitted a larger

photocurrent density in comparison with TSC under the applied potentials from -0.15 to -0.65 V, indicating that TSC/PDA possessed a better PEC performance and PDA could enhance the light absorption and trigger the photoelectrons transfer from the CB of TSC directly into the chelating PDA.

The IPCE spectra were a fundamental tool to elucidate the photoelectric behaviors of the photoactive materials by measuring the IPCE values at various wavelengths. Fig. 2B illustrated the corresponding outcomes according to Eq. (1)[36] with no bias voltage:

$$IPCE\% = \frac{1240 \times j}{\lambda \times P} \times 100 \qquad (1)$$

where λ was the wavelength (nm), j was the short circuit photocurrent density (mA cm^{-2}), and P was the incident light power (mW cm^{-2}). Notably, the TSC/PDA complex presented an improved photoresponse and higher IPCE value not only in ultraviolet region but also in the visible light region, which originated from the energy shift of the valence band in this complex.[22] Additionally, it was interesting to note that the maximum IPCE obtained with TSC/PDA associated with the wavelength had a phenomenon of redshift, further expending the utilization of the overwhole optical zone.

Subsequently, the typical open-circuit voltage (V_{oc}) changes of TSC and TSC/PDA films under visible light illumination were employed to evaluate their photoelectric performance (as shown in Fig. 2C). The V_{oc} represented the difference in Fermi level between photoactive material and counter electrode. In the dark, both TSC and TSC/PDA exhibited an initial Voc of -0.025 V, which suggested an accumulation of electrons on the films electrode.[37] When the light was on, most of the excited photoelectrons were collected, causing the shift of Fermi level to a more negative potential. Accompanied with the competition between electron accumulation and charge recombination, the Voc arrived at a stable state (maximum value) with the increase of photo-induced electrons under light irradiation. Once the light was cut off, the V_{oc} decayed as the collected electrons were relaxed owing to the scavenging by electron acceptor species in electrolyte and the recombination with photo-induced holes.[38] As expected, TSC/PDA presented a higher photovoltage and slower decay when light was cut on and off, which was due to the efficient utilization of the light as well as the low recombination rate of the excited e^{-}-h^{+} pair. The electron lifetime (τ) of TSC and TSC/PDA was calculated from the V_{oc} decay in dark according to the following Eq. (2).[39]

$$\tau = \frac{k_B T}{e}\left(\frac{dV_{OC}}{dt}\right)^{-1} \qquad (2)$$

where τ was the potential dependent lifetime, e was charge of a single electron, k_BT was the thermal energy in which T was the temperature in K and k_B was Boltzmann's constant. The dV_{oc}/dt was the derivative of the open-circuit voltage transient. The relationship between the electrons lifetime and Voc in TSC and TSC/PDA was presented in Fig. 2D. Obviously, TSC/PDA exhibited a longer decay lifetime of the accumulated electrons in comparison with TSC.

The aforementioned results affirmed that the TSC/PDA complex held higher photoelectric performance compared with the TSC due to their synergistic effect. These findings convincingly demonstrated that the self-assembled PDA by self-polymerization on TSC presented admirable sensitizing effect, which dramatically improved the PEC performance of the TSC and provided a prominent photocatalytic candidate for PEC biosensing.

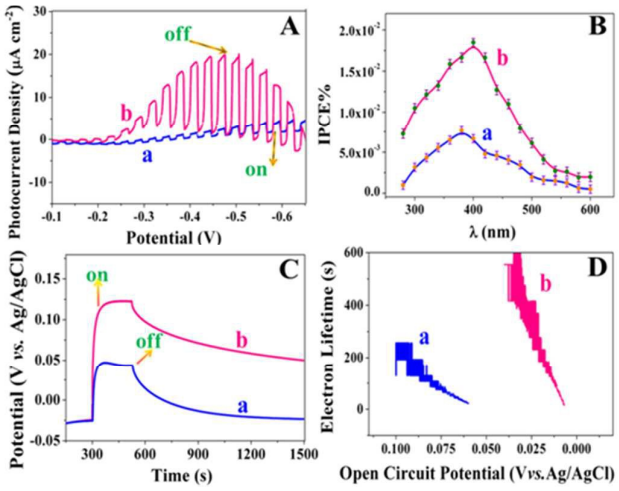

Figure 2 (A) Applied potential bias-dependent photocurrent densities, (B) IPCE spectra, (C) Voc time profile and (D) electron lifetimes measurements (determined from the Voc decay in dark) of (a) TSC and (b) TSC/PDA in 0.1M PBS (pH 7.0).

3.3 PEC biosensor characterization and detection strategy feasibility assay

The stepwise fabrication process of the immunosensor was monitored by PEC experiments and shown in Fig. 3A. Compared to the bare GCE (a), TSC modified electrode (b) presented an obvious cathode photocurrent signal under the applied potential of -0.3 V, revealing that TSC, as a new typical photoactive material, possessed tremendous potential for PEC biosensing applications. The generation of cathode photocurrent avoided the destructive effects of photo-generated holes to biomolecules. With the OMC coated on the GCE and then modified with TSC (curve c), the photocurrent intensity of the GCE/OMC/TSC increased significantly, which demonstrated that the OMC could trigger the rapid electrons transform in virtue of its excellent conductivity. While PDA was subsequently self-polymerized on the TSC films (curve d), the photocurrent intensity increased to 2.5 times higher than that of TSC/GCE on account of the fast photoelectrons moving from the CB of the TSC into the chelating PDA as well as the light absorption enhancement. Later on, the photocurrent intensity decreased gradually after the Ab anchoring and PSA@BMC specific binding (curves e and f). This could be attributed to the fact that the immobilization of these proteins owned weak charge-transfer abilities, suppressing the electrons transfer between the electrode and electrolyte. When GCE/OMC/TSC/PDA/Ab/PSA@BMC was immersed into the mixed solution containing HQ and H_2O_2, the photoresponse enhanced enormously in that BMC-initiated BCP reaction produced a strong oxidant (PBQ) by catalyzing the HQ. This in suit generated electron acceptor could receive photoelectrons form the LUMO of TSC/PDA, which further boosted the cathode photocurrent. Therefore, this PEC experiment preliminarily proved the successful fabrication of the immunosensor and the feasibility analysis for target tumor marker.

Another important tool for characterizing the interface properties of electrodes was also employed to investigate the assembly process of this PEC sensing platform. Fig. 3B showed the EIS impedance spectra of modified electrodes formed in progressive construction steps using $[Fe(CN)_6]^{3/4-}$ as the redox probe. Compared to naked GCE (curve a), the OMC modified electrode (curve b) exhibited a much smaller charge-transfer resistance (R_{ct}) owing to the admirable conductivity of OMC, which could be applied for enhancing the photoelectrons separation and transfer. With the TSC modified on GCE/OMC surface (curve c), the value of R_{ct} increased clearly due to the low conductivity of TSC, implying that the TSC was successfully deposited. However, after the self-polymerization with PDA, the R_{ct} reduced significantly (curve d), which could be elucidated as positively charged PDA with amino group supporting the transfer of negatively charged $[Fe(CN)_6]^{3-/4-}$. As expected, the semicircle was apparently enlarged after GCE/OMC/TSC/PDA matrix was soaked in Ab (e) and PSA@BMC (f) solution, which resulted from the nonconductive properties of Ab and the PSA. After the electrode of GCE/OMC/TSC/PDA/Ab/PSA@BMC was immersed into the HQ solution with the presence of H_2O_2, the measured R_{ct} was further increased due to the in suit generated PBQ film repelled the transfer of the negatively charged probe $[Fe(CN)_6]^{3/4-}$. Thus, the EIS characterization demonstrated that the proposed PSA biosensor was successfully fabricated.

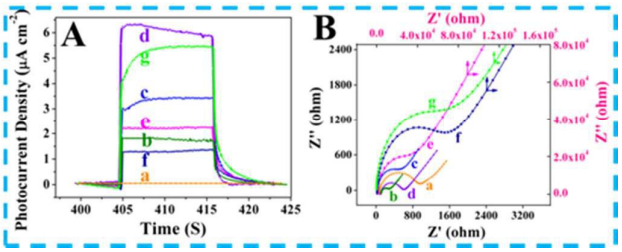

Figure 3 (A) PEC response and EIS spectra of different modified electrodes. (a) GCE; (c) GCE/OMC/TSC; (d) GCE/OMC/TSC/PDA; (e) GCE/OMC/TSC/PDA /Ab; (f) GCE/OMC/TSC/PDA/Ab/PSA@BMC; (g) GCE/OMC/TSC/PDA/Ab /PSA@BMC/PBQ. The (b) was GCE/TSC in pattern A and GCE/OMC in pattern B. The PEC tests were performed in 0.1 M PBS (pH 7.4) under the applied potential of -0.3 V. The EIS spectra were obtained in 5.0mmol/L $[Fe(CN)_6]^{3-/4-}$ solution containing 0.1mol/L KCl.

3.4 The tentative mechanism for the PSA detection

In this work, an exquisite competitive-type PEC biosensor was fabricated by accompanying the classical TSC photoactive materials co-sensitized with OMC and PDA as well as the BMC-initiated BCP reaction for improving the sensitivity of this designed platform. Under the applied potential of -0.3 V, the photoresponse of the TSC presented a cathode photocurrent. After the modification of OMC, the photocurrent density was higher than TSC, which was due to that the excellent electrical conduction of OMC was in favour of the fast electrons transfer from the external circuit to the valence band of the TSC, inhibiting the e^--h^+ pair recombination on TSC. When PDA was self-polymerized on the GCE/OMC/TSC films, the cathode photocurrent was further increased due to the more visible light harvesting and photo-generated charge carries separation. The formed TSC/PDA film possessed a more narrow band gap (~2.03 eV)[40] and a more negative CB (-1.29 eV), which promoted the light absorption rate and the complex owned stronger reducing capacity. Subsequently, anti-PSA was anchored on the OMC/TSC/PDA modified electrode using GLD as crosslinking agent. Then the GCE/OMC/TSC/PDA/Ab electrode was immersed into the mixed solution containing the PSA@BMC and PSA standards with different concentrations to facilitate the competition process. BMC, as a highly efficient peroxidase mimetic system, could catalyze the HQ to produce the PBQ precipitation, which could react with the photo-generated electrons from the CB of TSC. The photocurrent density decreased with the increase of PSA concentration because fewer PSA@BMC anchored onto the modified electrode surface, thus realizing the ultrasensitive detection of PSA.

3.5 Characteristics of the peroxidase-like activity of BMC

To further investigate the superiority of the proposed BMC inorganic nanocatalyst, the stability comparison between BMC and HRP in some special conditions was studied. As shown in Fig. 4A, both BMC and HRP exhibited a maximal photoresponse at the temperature of 30°C, however, in the whole range, the BMC showed a stronger catalytic performance than HRP. Additionally, BMC were significantly found to retain relatively stable catalytic activity even after treatment at 90 °C for 2 h in comparison with HRP. More inspiringly, the HRP inhibitors including ascorbate (AA), H_2O_2, sodium azide (NaN_3), sodium hydroxide (NaOH), and hydrochloric acid (HCl) had no obviously effect on catalytic activity of BMC, whereas they almost inhibited the activity of HRP completely (Fig. 4B). These outcomes indicated that BMC owned higher stability against the high temperatures and HRP inhibitors, which was suitable for developing ultrasensitive PEC immunoassays.

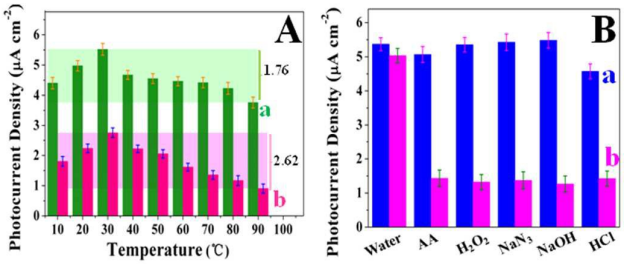

Figure 4 Catalytic activity of (a) BMC and (b) HRP: (A) after treatment for 2 h at different temperatures; (B) in the absence or present of ascorbic acid (AA), H_2O_2, NaN_3, NaOH and HCl (the concentration of HRP inhibitors was 5mM), respectively. Error bar represents the standard deviation (n=3).

3.6 Optimization of the PEC biosensing platform and experimental conditions

To achieve an optimal analytical performance for this design and enhance the competitive ability of the target PSA and BMC@PSA, the condition of the biosensing platform construction including the amount of OMC, TSC, and PDA. The optimal usage quantity was 3 mg/mL for both OMC and TSC (Fig. S1A and S1B, ESI†). As for PDA, the self-polymerization time of the GCE/OMC/TSC was 30 min (Fig. S1C, ESI†). In addition, some experimental conditions, such as incubation time for the immune-reaction, catalytic time for HQ by the enzyme mimetic, pH value, and the applied potential were investigated (Fig. S2, ESI†). Incubation time for Ab and PSA@BMC

were both 1h and the detection measurements were performed in PBS of pH 7.4 and applied potential of -0.3 V. The detailed explanation was submitted in supporting information.

3.7 Analytical performance of the biosensor

The PSA, one of the main clinical biomarkers for prostate cancer, was served as the model protein.[41] To evaluate the detectability of the PEC immunoassay, PSA standards with different concentration were tested on the basis of multifunctional PDA induced cathodic photocurrent increment and BMC initiated BCP reaction for altering the signal change. Under optimal conditions, the assay was carried out by utilizing Amperometric i-t curve in PBS solution (pH 7.4). As shown from Fig. 5A, the photocurrent density decreased with increasing PSA amounts. Fig. 5B demonstrated that the variation of photocurrent density linearly increased with the decreasing logarithm of target PSA concentration from 1×10^{-6} to 50 ng/mL with a detection limit (LOD) of 3.3 ng/mL. The regression equation could be fitted to j (μA cm^{-2}) = (-0.366±0.009)log C (ng/mL)+(2.671±0.03) with R^2=0.9952. Inspiringly, the detection range of this design was wider and the LOD was lower in comparison with other reported previously (Table S1, ESI†). Additionally, the feasibility of the strategy was investigated on real sample of human serum with the recovery rate of 99.14~106.8% (Table S2, ESI†).

Furthermore, the specificity of the PEC immunoassay toward the target PSA was examined by replacing of PSA with some possible interfering materials in human serum samples, including α-fetoprotein (AFP), carcinoembryonic antigen (CEA), and human Interleukin-6 (IL-6) with an excess hundred folds concentration of PSA. However, the detection signal of these interferences was lower than PSA (shown in Fig. 5C). Besides, the mixtures of these interferences with PSA all had no evident effect on PSA detection, revealing the high specificity of this multiple amplifying biosensor.

The reproducibility was another evaluation index for a newly developed analytical method. In this work, the relative standard deviation (RSD) was estimated by determining two different concentrations of PSA. Seven parallel replicate measurements of 0.001 ng/mL and 1.0 ng/mL were detected and the RSD were 1.98% and 2.16%, respectively. Additionally, the long-time stability was measured and there was no obvious photocurrent deterioration (maintaining 92.6% of the initial result) after ten days storage at 4 °C. The above outcome suggested that the constructed biosensor could be used in clinical and biological applications for ultrasensitive PSA determination.

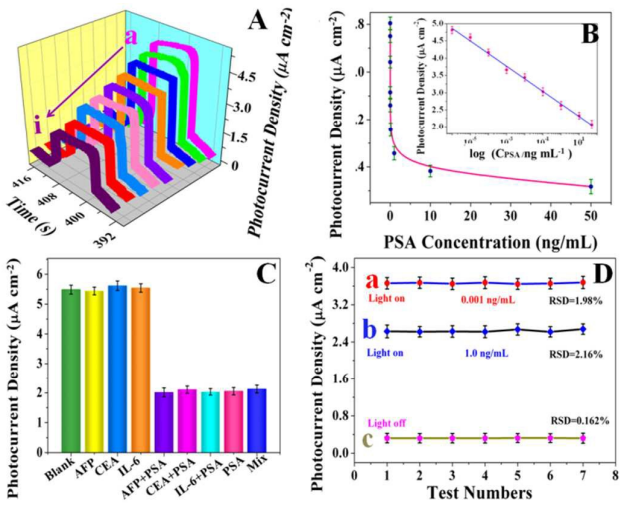

Figure 5 (A) The photocurrent density of different PSA concentrations (a–i) 10^{-6}, 10^{-5}, 10^{-4}, 10^{-3}, 10^{-2}, 0.1, 1.0, 10, and 50ng/mL. (B) The corresponding calibration curve. (C) The photocurrent densities of the prepared sensor to PSA with interfering agents, including 50ng mL-1 AFP, CEA and IL-6, 0.1 ng/mL PSA and the corresponding mixed solutions. (D) The reproducibility by detecting different PSA concentration: (a) 0.001ng/mL, (b) 1.0ng/mL, (c) dark current response without light irradiation.

Conclusions

In summary, a new-type PEC biosensing platform based on OMC and PDA co-sensitized TSC as well as the signal amplification effect of BMC labeling was developed. The classical photoactive material of TSC with fine photoelectric efficiency was first applied for PEC immunoassay. With the support of OMC, the cathode photocurrent originated from TSC increased significantly under the bias voltage of -0.3 V. Introduction of PDA on TSC film not only strengthened the visible light absorption and enhanced cathode photocurrent conversion efficiency, but also employed as an appropriate matrix for immobilizing Ab. In the competitive progress, BMC labeled PSA competed with the target PSA for specific binding the Ab, and the photoresponse was reinforced once again, mainly resulted from the in suit generated electrons accepter induced by BMC-initiated BCP reaction. These characteristics endowed the PEC immunosensor with high sensitivity, representing a ubiquitous strategy with large potential in the field of clinical diagnostics and prognosis.

Acknowledgements

This project was financially supported by the NSFC (21205016, 21575024), National Science Foundation of Fujian Province (2011J05020), and Education Department of Fujian Province (JA14071, JB14036, JA13068).

Notes and references

1 W. W. Zhao, Z. Y. Ma, P. P. Yu, X. Y. Dong, J. J. Xu and H. Y.Chen, *Anal. Chem.*, 2012, **84**, 917-923.

2 B. Acevedo, Y. Perera, M. Ruiz, G. Rojas, J. Benítez, M. Ayala and J. Gavilondo, *Clin. Chim. Acta*, 2002, **317**, 55-63.

3 Z. Gao, M. Xu, M. Lu, G. Chen and D. Tang, *Biosens. Bioelectron.*, 2015, **70**, 194-201.

4 P. Jolly, V. Tamboli, R. L. Harniman, P. Estrela, C. J. Allender and J. L. Bowen, *Biosens. Bioelectron.*, 2016, **75**, 188-195.

5 G. Ertürk, H. Özen, M. A. Tümer, B. Mattiasson and A. Denizli, *Sens. Actuators, B*, 2016, **224**, 823-832.

6 Y. T. Chen, L. P. Tuan, H. W. Chen, I. A. Wei, M.-Y. Chou, H.-M. Chen, Y. C. Tyan and S. F. Chen, *Anal. Chem.*, 2015, **87**, 545-553.

7 R. Simon, S. Passeron, J. Lemoine and A. Salvador, *J. Chromatogr. A*, 2014, **1354**, 75-84.

8 W. W. Zhao, Z. Y. Ma, D. Y. Yan, J. J. Xu and H. Y. Chen, *Anal. Chem.*, 2012, **84**, 10518-10521.

9 W. W. Zhao, J. J. Xu and H. Y. Chen, *Chem. Soc. Rev.*, 2015, **44**, 729-741.

10 W. W. Zhao, J. J. Xu and H. Y. Chen, *Chem. Rev.*, 2014, **114**, 7421-7441.

11 G. L. Wang, K. L. Liu, J. X. Shu, T. T. Gu, X. M. Wu, Y. M. Dong and Z. J. Li, *Biosens. Bioelectron.*, 2015, **69**, 106-112.

12 G. L. Wang, X. F. Xu, L. Qiu, Y. M. Dong, Z. J. Li and C. Zhang, *ACS Appl. Mater. Interfaces*, 2014, **6**, 6434-6442.

13 W. W. Zhao, X. Y. Dong, J. Wang, F. Y. Kong, J. J. Xu and H. Y. Chen, *Chem. Commun.*, 2012, **48**, 5253-5255.

14 W. W. Zhao, J. Wang, Y. C. Zhu, J. J. Xu and H. Y. Chen, *Anal. Chem.*, 2015, **87**, 9520-9531.

15 W. W. Zhao, P. P. Yu, J.-J. Xu and H. Y. Chen, *Electrochem. Commun.*, 2011, **13**, 495-497.

16 G. L. Wang, J. X. Shu, Y. M. Dong, X. M. Wu and Z. J. Li, *Biosens. Bioelectron.*, 2015, **66**, 283-289.

17 W. Zhang, Y. Tang, J. Liu, Y. Ma, L. Jiang, W. Huang, F.-w. Huo and D. Tian, *J. Mater. Chem. B*, 2014, **2**, 8490-8495.

18 E. Tsuji, K. i. Fukui and A. Imanishi, *Journal of Physical Chemistry C*, 2014, **118**, 5406-5413.

19 W. Jiao, L. Wang, G. Liu, G. Q. Lu and H.-M. Cheng, *Acs Catalysis*, 2012, **2**, 1854-1859.

20 Y. Shuang, Y. Hou, B. Zhang and H. G. Yang, *Chem. Eur. J.*, 2013, **52**, 4098-4102.

21 D. H. Kim, W. S. Kim, S. B. Lee and S. H. Hong, *Sens. Actuators, B*, 2010, **147**, 653-659.

22 T. Rajh, L. X. Chen, K. Lukas, T. Liu, M. C. Thurnauer and D. M. Tiede, *J. Phys. Chem. B*, 2002, **106**, 10543-10552.

23 S. M. D. Haeshin Lee, William M. Miller, Phillip B. Messersmith, *Science*, 2007, **318**, 426-430.

24 Y. Fu, P. Li, T. Wang, L. Bu, Q. Xie, X. Xu, L. Lei, C. Zou, J. Chen and S. Yao, *Biosens. Bioelectron.*, 2010, **25**, 1699-1704.

25 W. Wang, R. Li, M. Tian, L. Liu, H. Zou, X. Zhao and L. Zhang, *ACS Appl. Mater. Interfaces*, 2013, **5**, 2062-2069.

26 R. Li, J. Gao, P. Gao, S. Zhang, Y. Liu, B. Du and Q. Wei, *New J. Chem.*, 2015, **39**, 731-738.

27 J. S. Yu, S. Kang, S. B. Yoon and G. Chai, *J. Am. Chem. Soc.*, 2002, **124**, 9382-9383.

28 X. Peng, D. Huang, T. Odoom-Wubah, D. Fu, J. Huang and Q. Qin, *J. Colloid Interface Sci.*, 2014, **430**, 272-282.

29 C. A. Chen, K. Y. Chen, Y. S. Huang, D. S. Tsai, K. K. Tiong and F. Z. Chien, *J. Cryst. Growth*, 2008, **310**, 3663-3667.

30 G. Zeng, K. K. Li, H. G. Yang and Y. H. Zhang, *Vib. Spectrosc.*, 2013, **68**, 279-284.

31 H. Xu, P. Reunchan, S. Ouyang, H. Tong, N. Umezawa, T. Kako and J. Ye, *Chem. Mater.*, 2013, **25**, 405-411.

32 Y. Li, H. Zhang, Z. Guo, J. Han, X. Zhao, Q. Zhao and S. J. Kim, *Langmuir*, 2008, **24**, 8351-8357.

33 J. Tang, J. Li, P. Da, Y. Wang and G. Zheng, *Chem. Eur. J.*, 2015, **21**, 11288-11299.

34 S. Yotsumoto Neto, R. d. C. S. Luz and F. S. Damos, *Electrochem. Commun.*, 2016, **62**, 1-4.

35 N. M. Dimitrijevic, E. Rozhkova and T. Rajh, *J. Am. Chem. Soc.*, 2009, **131**, 2893-2899.

36 A. Kongkanand, K. Tvrdy, K. Takechi, M. Kuno and P. V. Kamat, *J. Am. Chem. Soc.*, 2008, **130**, 4007-4015.

37 X. M. Song, J. M. Wu, M. Z. Tang, B. Qi and M. Yan, *J. Phys. Chem. C*, 2008, **112**, 19484-19492.

38 Q. Chen, H. Liu, Y. Xin, X. Cheng and J. Li, *Appl. Surf. Sci.*, 2013, **264**, 476-484.

39 B. H. Meekins and P. V. Kamat, *ACS Nano*, 2009, **3**, 3437-3446.

40 H. J. Nam, B. Kim, M. J. Ko, M. Jin, J. M. Kim and D. Y. Jung, *Chem. Eur. J.*, 2012, **18**, 14000-14007.

41 L. Deng, H. Y. Chen and J. J. Xu, *Electrochem. Commun.*, 2015, **59**, 56-59.

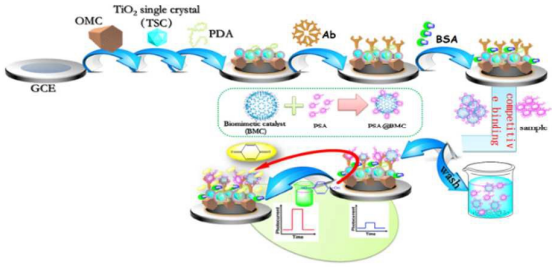

A photoelectrochemical protocol was designed for quantitative monitoring the tumor markers by utilizing the poly(dopamine)-sensitized titanium TiO_2 signal crystal.